

# Permanent Magnet Spiral Motor for Magnetic Gradient Energy Utilization: Axial Magnetic Field

Thomas F. Valone

*Integrity Research Institute*  
5020 Sunnyside Avenue, Suite 209  
Beltsville, MD 20705  
301-220-0440, [IRI@starpower.net](mailto:IRI@starpower.net)

**Abstract.** The Spiral Magnetic Motor, which can accelerate a magnetized rotor through 90% of its cycle with only permanent magnets, was an energy milestone for the 20th century patents by Kure Tekkosho in the 1970's. However, the Japanese company used old ferrite magnets which are relatively weak and an electrically-powered coil to jump start every cycle, which defeated the primary benefit of the permanent magnet motor design. The principle of applying an inhomogeneous, anisotropic magnetic field gradient force  $F_z = \mu \cos \varphi dB/dz$ , with permanent magnets is well-known in physics, e.g., Stern-Gerlach experiment, which exploits the interaction of a magnetic moment with the aligned electron spins of magnetic domains. In this case, it is applied to  $dB/d\theta$  in polar coordinates, where the force  $F_\theta$  depends equally on the magnetic moment, the cosine of the angle between the magnetic moment and the field gradient. The radial magnetic field increases in strength (in the attractive mode) or decreases in strength (in the repulsive mode) as the rotor turns through one complete cycle. An electromagnetic pulsed switching has been historically used to help the rotor traverse the gap (*detent*) between the end of the magnetic stator arc and the beginning (Kure Tekko, 1980). However, alternative magnetic pulse and switching designs have been developed, as well as strategic eddy current creation. This work focuses on the switching mechanism, novel magnetic pulse methods and advantageous angular momentum improvements. For example, a collaborative effort has begun with Toshiyuki Ueno (University of Tokyo) who has invented an extremely low power, combination magnetostrictive-piezoelectric (MS-PZT) device for generating low frequency magnetic fields and consumes "zero power" for static magnetic field production (Ueno, 2004 and 2007a). Utilizing a pickup coil such as an ultra-miniature millihenry inductor with a piezoelectric actuator or simply Wiegand wire geometry, it is shown that the necessary power for magnetic field switching device can be achieved in order to deflect the rotor magnet in transit. The Wiegand effect itself (bistable FeCoV wire called "Vicalloy") invented by John Wiegand (Switchable Magnetic Device, US Patent #4,247,601), utilizing Barkhausen jumps of magnetic domains, is also applied for a similar achievement (Dilatush, 1977). Conventional approaches for spiral magnetic gradient force production have not been adequate for magnetostatic motors to perform useful work. It is proposed that integrating a magnetic force control device with a spiral stator inhomogeneous axial magnetic field motor is a viable approach to add a sufficient nonlinear boundary shift to apply the angular momentum and potential energy gained in 315 degrees of the motor cycle.

**Keywords:** Magnetic Gradient, Spiral Magnet, Inhomogeneous Magnetic Field, Piezoelectric-Magnetostrictive, Magnetic Pulse Control, Magnetostatic Energy Density, Axial Magnetic Field  
**PACS:** 75.50.Ww, 75.30.Gw, 77.65.-j

## INTRODUCTION

Kure Tekkosho in the 1970's, Figure 1, secured a number of Japanese patents directed toward a spiral set of magnets, a Spiral Magnetic Motor (SMM) that can accelerate a magnetized rotor. However, the Japanese company used old ferrite magnets which possess a relatively weak coercive force and an additional electrically-powered coil which defeated the purpose of the motor design. Therefore, its Magnetic Wankel was not a successful attempt at a self-powered motor (Scott, 1980). The principle is a magnetic gradient that is analogous to the geographic gravity gradient where a steeper incline (higher gradient) provides a higher speed for vehicles going downhill. Such a magnetic field varying spatially is also found in a linear track (Arrott, 2006).

As with the Stern-Gerlach physics experiment to separate spinning protons, the magnetic field is stronger at one end of the track, whether it is linear or circular with an inhomogeneous magnetic field. The equation for the linear magnetic gradient force, equation (1), depends upon the cosine of the angle  $\phi$  between the magnetic moment  $\mu_s$  and the direction of the gradient of the magnetic field (Gautreau, 1978). As an aside, Gautreau gives the subscript s to the magnetic moment symbol used here since it is associated with the intrinsic angular momentum S of the electron.

$$F_z = \mu_s \cos \phi \frac{dB}{dz} \quad (1)$$

An example of a linear magnetic gradient force is in Hartman's US patent #4,215,330 which moves a steel ball bearing up a 10 degree incline with permanent magnet gradient force, Figure 2. The applications for a successful completion of this proposed prime mover fall into two basic categories but others may be discovered at a later time: The first category is the production of electrical power, replacing fossil-fuel based generation, for a Magnetic Microturbine. The second category is the production of torque for automobile engines and basic transportation with a Magnetic Car. Both applications will free the countries of the world from dependence on oil and natural gas, thus raising the standard of living for everyone, especially in the third world, while being a clean energy source, once an efficient magnetic switching mechanism is achieved.

The Spiral Magnetic Motor invented by the Kure Tekkosho Co. (Ono Gunji, "Permanent Magnet Prime Mover," JP55144783) has remained an Electrically-Stimulated Linear Induction Motor (ESLIM) but also utilizing a little known physics principle called the permanent magnet "magnetic gradient force." Though there have been incremental improvements over the past thirty years, since this investigator became aware of the invention, no scientific investigation into the feasibility of a true magnetic motor (without electric assist) has been made until now. Permanent magnet motors that try to achieve unusual coefficients of performance with changes in magnetic geometry, switching reluctance schemes and various magnetic configurations generally have not been successful in developing an LIM that is driven solely by magnetic energy. There are some designs that should be regarded as conventional and others as promising in the search for a true magnetic motor that is entirely powered by the magnetic gradient force. It is proposed that a MAGnetic Linear Induction Motor (MAGLIM) is inevitable with the application of proper engineering principles, *since magnetic field switching is now easier than ever.*

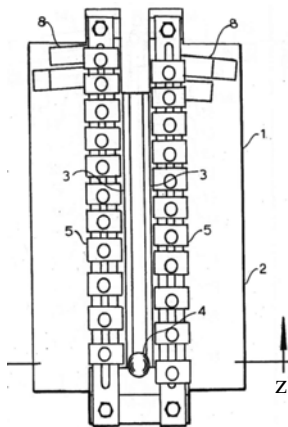


**FIGURE 2.** Magnetic gradient force in Hartman's US patent #4,215,330.

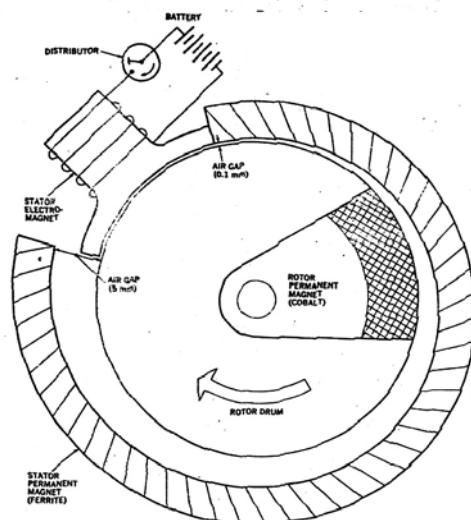


**FIGURE 1.** Kure Tekko "Magnetic Wankel" running in repulsive mode

The generation of inhomogeneous magnetic fields in a linear direction forming a magnetic gradient is a crucial feature of the proposed MAGLIM. It also is well-known magnetostatics and a promising area of research as explained in the references to textbook physics principles.

The linear magnetic gradient force proportional to  $dB/dz$  displayed in Figure 2 (with z pointing to the top of the page) is converted to  $dB/d\theta$  in the circular case, equation (2), utilized in this paper, where M is the macroscopic magnetic moment and  $\phi$  is the angle between M and B. Taking the diagram of Figure 1, a radial magnetic field decreases its attraction as the rotor turns through one complete cycle. A large electromagnetic pulsed switching is usually needed, as was used in Figure 1 and in two of the recent patents awarded to H. Paul Sprain (Apparatus and Process for Generating Energy, US Patents #6,954,019, 2005 and #7,265,471) to help the rotor traverse the gap (detent) between the end of the magnetic spiral stator arc and the beginning of the arc.

$$F_\theta = M \cos \phi \frac{dB}{d\theta} \quad (2)$$

## SPIRAL MAGNET MOTOR CONSIDERATIONS

In this paper, *axial* magnetic field orientation is experimentally explored as a matter of convenience. Simulation with FEMM also indicated that a transverse field was of higher density with the axial magnet (parallel magnets of opposite poles) than the radial magnetic field design with opposite poles, perhaps because radial magnets in the attraction mode have a very strong radial field and low transverse (circumferential) field. A second part to this paper will be published by this author on *radial magnetic field* orientation SMM designs, which is more difficult to engineer but achieves a stronger coupling. As a design criterion, the moving magnetized rotor in the Spiral Magnetic Motor needs to be modeled as a *changing magnetic field* ( $dB/dt$ ) with regard to the stator as well.

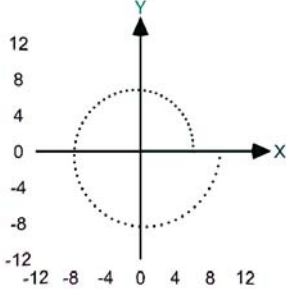


**FIGURE 3.** Example of Archimedean spiral for SMM stator magnets with  $r = 6 + \theta/2$ .

An example of one of the Archimedean spirals that was used in these experiments is in Figure 3. The equation of the stator spiral, in polar coordinates is  $r = 6 + \theta/2$ . A dotted plot with Reuniter Ver. 2.6, was used to facilitate precise cylindrical magnet placement for the axial stator magnets. Other spirals were also compared to maximize the circumferential force  $F_\theta$  to achieve the highest revolution speed and in some cases (e.g., 1.25" and 3" rotor designs), for the rotor to completely counteract gravity when the plane of the wooden or acrylic stator was placed vertically, as in Figure 3, with the Y-axis upwards.

With the Archimedean spiral of Figure 3, the basic equation for the radial component of the linear magnetic field can be written in cylindrical coordinates as  $B_r = r + n(\theta)$  where (theta) is in radians. Plotting such a *linear relationship*, the magnetic gradient (slope) is simply  $n$ , where  $n = dB/d\theta$ . It is conceivable that a parabolic  $B_r = a(\theta)^2 + b(\theta)$  or even exponential relationship  $B_r = ae^\theta$  may be theoretically simulated and experimentally tested in the future. These relationships would provide a higher magnetic gradient at the exit point where  $\theta = 2\pi$  radians which could increase the peak kinetic energy of the rotor. Placing the stator magnets slightly closer together near the end of the spiral has also been found to speed the rotor up near the end of its cycle and increase its kinetic energy slightly, thus applying a nonlinear magnetic gradient.

### Spiral Magnetic Motor Energy Balance

The idealized linear relationship of B and rotation angle was realized in the Sprain motor project (2-03-04 HPS data), for which this investigator was a consultant. The magnetic gradient, using ferrite magnets, was  $dB/d\theta \cong 100$  Gauss/rad. Of course, the torque can be theoretically calculated from the classical equation  $T = r \times F$  with the force related to the magnetic potential energy by  $F = \nabla U$  where  $U = M \cdot B$  and M equals the magnetic moment, also known as the magnetic dipole moment (Halliday, 1968). However, the force F is really a trigonometric vector sum of the tangential acceleration and the centripetal acceleration, made only more complicated by the surface magnetic field distribution and relative coupling between rotor and stator. In other words, the attempt to simplify the interaction to a simple dot product of the magnetic dipole and the magnetic flux density can only agree experimentally where there is a point dipole and a homogeneous magnetic field. Neither of these conditions exists in the ESLIM or MAGLIM configuration.

It is an educational exercise, however, to follow through with the standard energy balance of kinetic and potential energy. When taking the gradient of the dot product above to find the force F, the result is actually

$$F = \frac{M}{r} \frac{\partial B_r}{\partial \theta} + M \frac{\partial B_r}{\partial r} \quad (3)$$

The partial derivative  $\partial B_r / \partial r$  can be argued to be equal to zero because the motion of the rotor is only in the circumferential direction ( $\theta$ ) and only uniform, permanent magnets are used in the stator. Torque applied to the rotor ( $T = r \times F$ ) with  $r$  and  $F$  perpendicular ( $\sin \theta = 1$ ), is simply

$$T = M \frac{\partial B_r}{\partial \theta} \quad (4)$$

A radial magnetic design is suggested by the term  $\partial B_r / \partial \theta$  which *should be maximized for optimum torque production*. As we revisit the calculation for potential energy  $U$ , it is apparent that the dot product becomes

$$U = M_r B_r + M_\theta B_\theta \quad (5)$$

However, the magnetic moment of an axially or radially magnetized rotor should have a zero  $\theta$  component that will make  $M_\theta$  also zero. The conclusion of all of the preceding physics leads to the classical work-energy calculation  $W = F \cdot dx$ , which for rotation about a fixed axis becomes (Halliday, 1968)

$$W = \int T \cdot d\theta = \int M \, dB_r \quad (6)$$

Since  $M$  is a constant for a given magnet, the change of the magnetic field over a cycle from 0 to  $2\pi$  is thus determined to be the only variable that contributes to the work done in the SMM. The experimental measurements for radial magnetic field variation will be included in the second part to this paper, since only axial magnetic field rotors and stators were used in this part.

The usual method is to set the work equal to the kinetic energy  $\frac{1}{2}I\omega^2$  where the moment of inertia  $I = \frac{1}{2}mr^2$  for a cylinder but in the case of ESLIM, it is circular reasoning. Though parameters can be calculated in this manner, no new fundamental information about the open system energy input is produced with this classical approach.

As an alternative insight into magnetic field energy, the maximum electrostatic field energy density can be compared to the magnetostatic field energy density for reasonable field intensities available today (Niarchos, 2003). The maximum electric field that can be applied in experimental circumstances in air is approximately 3 MV/m. Therefore, the maximum electrostatic energy density that can be expected to be available is

$$U_E = \frac{1}{2} \epsilon_0 E^2 \quad (7)$$

where  $\epsilon_0$  is the permittivity of free space and  $E$  is the electric field (3 MV/m), giving an electric energy density on the order of 40 J/m<sup>3</sup>. However, today NdFeB magnets, grade N52, have approached the maximum flux density that iron theoretically possesses: approximately 20 kG or 2 T which gives, using the permeability  $\mu_0$  of free space, a magnetostatic potential energy density of

$$U_B = \frac{1}{2} B^2 / \mu_0 \quad (8)$$

which equals approximately 2 MJ/m<sup>3</sup> which is about 50,000 times the available energy density of electric fields. This shows why magnetostatic interactions dominate for macro-world power production.

A separate paper is being co-authored on the theoretical quantum mechanical basis of magnetism in order to include the contribution from zero point energy, the Bohr magneton and the coupling of electron spin to the quantum vacuum. The orbital angular momentum of the electron contributes very little (less than 2%) to magnetism, while spin angular momentum is the primary source of microscopic magnetism (Chikazumi, 1964). The derivation of the total energy of a magnetic system given by the sum of the magnetostatic energy and the anisotropy energy due to the rotation of spins which is gained from the angular momentum of the vacuum is the basic thesis. Thus, the energy source of magnetic-powered devices will no longer be mysterious or elusive. Certainly energy physics has to be considered and evaluated in the operation of ESLIM or the proposed MAGLIM. Though classical physics does not provide a satisfactory explanation for the possibility of a self-sustained operation for either design, even with an open system, quantum physics offers a rigorous consideration of the angular momentum contribution from the quantum vacuum to electron spin, the main contributor to ferromagnetism (Valone, 2008).

## Halbach Magnet Arrays

Examining linear induction motors (LIMs), the Halbach array is used (rotating magnetic domains assembled together) to provide a “superior magnetic flux property.” Halbach arrays demonstrate the ability to create magnetic fields on only one side of the array (in this case, the downside). Seen in the diagram in Figure 4 the standard mover with (a) the vertical magnetization (up and down) is compared to the (b) Halbach array style which provides a *tighter coupling and stronger attraction* between the mover and stator. The Halbach array also induces a dB/dt term since the changing magnetic field direction appears as a time-dependent rotating magnetic field to the mover. This also allows a resonant frequency design to be implemented into the mechanical assembly of magnets as well. The science of linear motors has progressed significantly in the past few decades due to the heroic efforts of the late Professor Eric Laithwaite of Queens College, London who perfected magnetic levitation (MAGLEV) for commercial train applications (Laithwaite, 1970; Valone, 2002). Reviewing Figures 4 and 5, we see some of these LIM design techniques of Laithwaite’s that are used to enhance the performance capability in the MAGLIM.

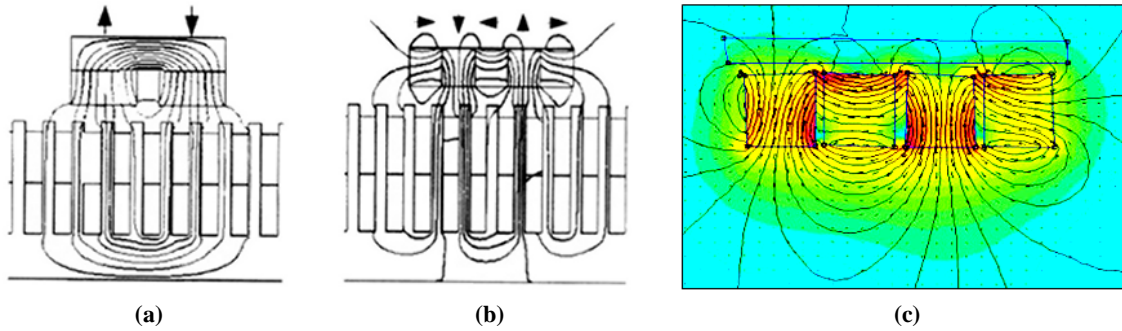


**FIGURE 4.** Typical (a) horseshoe magnet above a LIM stator, where arrows indicate the magnetic field direction, versus the (b) Halbach array above a LIM, showing the higher field intensity present, and (c) a FEMM simulation of a Halbach array, showing the asymmetry of flux lines.

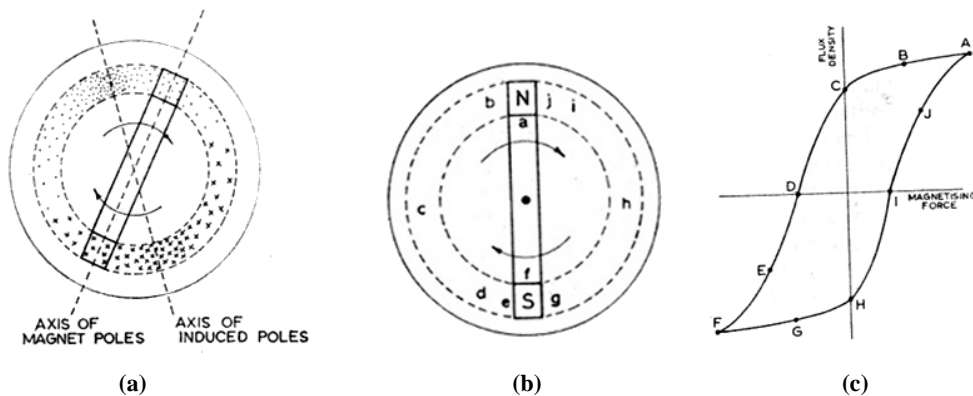


**FIGURE 5.** Prof. Laithwaite’s “Hysteresis Motor” creates delayed eddy currents based on the type of metal plate: (a) shows like poles formed below and behind bar magnet rotor; (b) and (c) show the points on the B-H curve corresponding to certain hysteresis points on the metal plate during the rotation cycle.

For the past ten years, modern high strength NdFeB magnets are providing a lightweight alternative to electromagnets for “on-board magnetic field sources” in a magnetic levitation vehicle. Therefore, the trend is toward more NdFeB Halbach arrays (Hoburg, 2004).

The magnetic fields in Halbach array “rotate” 90° from one magnet to the other, as it passes over the stator in Figure 4b, in order to accomplish two separate purposes:

- a) to create fields that *vary periodically* with space in the direction of travel of the vehicle, with a dominant first Fourier component;
- b) to put nearly all of the field either above or below the array, so as to *maximize the strength of the field* that interacts with the track (stator).

It is suggested that Halbach arrays can be an important addition to the rotor design of MAGLIM, where they can be added radially to the ends of the radially oriented magnet rotors. If Halbach arrays were used in the axial magnet orientation design, it is proposed that a few layers of soft iron shielding at the end of the spiral stator will produce a dramatically reduced detent and increased overshoot.

### Hysteresis Magnetic Motor and Favorable Eddy Currents

Another fascinating technique that utilizes Lenz’s Law which opposes any changing magnetic field is the magnetization effect on a metal plate with a particularly favorable permeability that improves and propels the magnetic rotor, which is of the same design as ESLIM (Laithwaite, 1970). Called the *Hysteresis Motor* (Figure 5), it

is designed to have a bar magnet parallel to the rotor with North and South pole radially oriented on the rotor. The important trick is to add a low permeability metal plate underneath the rotor that becomes momentarily magnetized due to Lenz's Law during the passage of the rotor over it. Favorable repulsive magnetic fields (like poles) form behind the rotor *as long as the eddy current formation time for that metal is of the same order of magnitude as the speed of the rotor*. As seen in the diagram, each of the induced poles in the steel "carries a high flux density" and pushes the rotor further away, "giving the effect of a pair of permanent magnet poles which are displaced from the position of the driving poles." Perhaps the conclusion to this design is the most compelling for MAGLIM: "This condition is therefore suitable for the production of continuous torque, without further relative motion between magnets and disc and the machine can run synchronously on the residual magnetism effect" (Laithwaite, 1970). The Hysteresis Motor may use axially magnetized poles (perpendicular to the disc) or radial magnets as in Figure 5(a), as well as custom L-shaped magnets in the MAGLIM to achieve a dual effect from the stator and the disc.

Seen in Figure 5 is the design effect of the rotor and disc with the typical hysteresis curve (B-H curve) which is now impressed onto the disc during dynamic motion. An interesting variation of the motor is the "Rack and Pinion" type of hysteresis motor that combines the teeth or slots of Figure 4 that make up the rack of a standard LIM with the magnetized rotor of Figure 5.

Since the rotor is moving, there is a delay in the Lenz' Law effect that creates like poles BEHIND the rotor pole, which normally tries to *oppose* the build-up of magnetic field intensity in the disc. The like magnetic pole then PUSHES the two away from each other but only if it has a delayed reaction. The governing equation, undisclosed by Laithwaite, but uncovered by this investigator, is due to a time lag for corresponding induction, derived from the same equation used in the theory of diffusion with  $\rho/4\pi\mu$  as the diffusion constant. In series form, MacColl's equation for *a build-up of flux in sheets subjected to a sudden change of field* has a first term,

$$\frac{B}{\mu H} = 1 - \frac{8}{\pi^2} e^{-\beta t} \quad (9)$$

with  $t$  = time (sec) and

$$\beta = \pi\rho / (4\mu\delta^2) \quad (10)$$

where  $\rho$  = resistivity,  $\mu$  = permeability,  $\delta$  = thickness of plate, with a field  $H$  suddenly applied (Bozorth, 2003).

The SMM fits this equation fairly well since the angular velocity was estimated to be on the order of a revolution per second (1 RPS = 1 Hz) from five different spiral motors that were constructed and tested. Therefore, if the build-up of the opposing eddy current field is on the order of a tenth of a second, it is likely to be suitable for a delayed response of eddy currents that would be favorable. It has been found by this investigator that by choosing aluminum or copper for example, the permeability will be the same as free space ( $\mu_o = 4\pi \times 10^{-7}$ ), which is very low and the resistivity is also low. Choosing an aluminum plate that is about a centimeter (1 cm) thick would also be a good choice since the thickness of the sheet "delta" is squared and also in the numerator. Altogether, the calculation shows a relatively *slow build-up over a tenth of a second* and only about 30% at a millisecond after the stator field magnet is applied to the rotating disk, which is in keeping with a delayed eddy current predicted by Laithwaite that will push the rotor along.

## **MAGNETOSTRICTIVE-PIEZOELECTRIC PULSER FOR DETENT NEUTRALIZATION**

For years, an electromagnet has been the only detent neutralizer used for the ESLIM, Figure 1, for the purpose of producing a pulsed magnetic field that cancels the end field with an expenditure of 150 watts for 0.040 seconds (6 Joules of energy, 12-12-02 H.P. Sprain data). Such a process is also theoretically referred to as regauging or changing boundary conditions suddenly. Recently, new improvements to switching magnetic fields have become available for low frequency applications (Ueno, 2003). As seen in Figure 6, a new combination of a giant magnetostrictive (MS) rod with a piezoelectric (PZT) actuator invented only a couple of years ago creates a remarkably efficient effect for static or dynamic operation. The MS-PZT magnetic field generator *consumes no power* to maintain a static magnetic field and also demonstrates a 77% energy savings (0.27 W vs. 1.2 W) for dynamic pulsed magnetic field production up to about 10 Hz (600 RPM) and even higher for 1 Hz (60 RPM) or lower, in the range where ESLIM operates (Ueno, 2007b). This is the primary innovative concept of this investigator that the old-fashioned pulse coil for ESLIM be replaced with this MS-PZT device for a possible solution to the proposed MAGLIM.

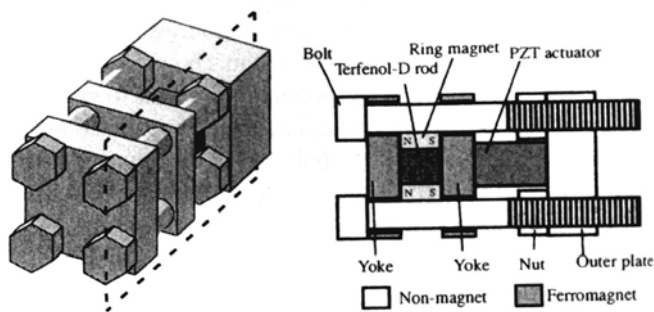


FIGURE 6. Magnetostrictive and piezoelectric (MS-PZT) combination in a vise creates pulsed magnetic fields with surprisingly little energy input.

COMPARISON OF POWER CONSUMPTION OF ELECTROMAGNET AND DEVICE IN STATIC AND DYNAMIC OPERATION

	E.M.	Device
<b>Static operation</b>		
Max input voltage [V]	2	200
Power consumption [W]	3.0	0.0
<b>Dynamic operation (10Hz)</b>		
Max input voltage	2	200
Power consumption	1.2	0.27
<b>Dynamic operation (100Hz)</b>		
Max input voltage	2	200
Power consumption	1.2	2.47

FIGURE 7. Energy consumption for the MS-PZT (Device) as compared to an electromagnet. Note the device has zero power consumption in the static case due to the charge storage capability of piezoelectric transducers.

### Wiegand Pulse Generator

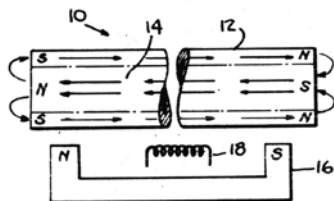


FIGURE 8. A two-layer Wiegand wire with pickup coil.

An additional discovery by this investigator that could regauge or recharge the rotor at the end of each cycle is the use of a Wiegand pulse generator to produce a magnetic pulse solely powered by Barkhausen effect caused by the passing magnetic field, *without recoil of any kind* (Figure 8). Naturally, the energy consideration of switching microscopic magnetic domains (0.1 mm) is an important part of such a treatment but beyond the scope of this paper. The *Barkhausen effect* is defined as the collective, sudden alignment of magnetic domains (Barkhausen, 1919) which can be heard by using a magnetic pickup coil speaker or microphone. This led to a surprisingly important effect that this investigation has uncovered: a Wiegand module with a coil surrounding it or even a bare ultra-miniature induction coil could power the MS-PZT without any

external electricity input of any kind utilizing the changing magnetic field of the passing rotor. Barkhausen discovered that certain materials like Permalloy, if wound with a wire, create a voltage pulse, just like a coil exposed to a momentary magnetic field, as the magnetic domains shift together to align themselves with the field. In 1973, John Wiegand patented a breakerless ignition system (# 3,757,754) as seen in Figure 8. The improved wires called Vicalloy, subsequently made by Wiegand Electronics and now a host of other manufacturers, generate 12 V to 16 V (with a coil wound around the wire) without any electrical input and can easily conduct through 1000 feet of 24-gauge wire, producing several milliwatts of power. They are already used in keyless door opening locks in hotels and in a host of other applications worldwide, without batteries of any kind. In Figure 8, it is proposed that the rotor (16) can draw close to a bundle of Wiegand wires (14) or a larger, custom-designed Wiegand rod, at the end of the spiraled stator track and coil (18) necessary to trigger the MS-PZT pulsed magnetic field.

Wiegand designed the wire (10) in Figure 8 to have a low coercivity core (14) and high coercivity shell (12) for resetting the magnetic alignment for another pulse cycle from a passing magnet (16). Coil 18 can be added for a desired voltage output pulse if required.

### Piezoelectric Actuators Lift Oranges

Piezoelectric actuators called “piezo-composites” licensed by NASA are also available to quickly and effectively displace a stator magnet with a range of 1000 in-lb/in<sup>3</sup> using only voltage pulses and virtually no current (Smart Material Corp., Sarasota FL, [www.smart-material.com](http://www.smart-material.com), d31 type P2). The Macro Fiber Composite (MFC) is an innovative actuator that offers high performance and flexibility in a cost-competitive device. The MFC consists of rectangular piezo ceramic rods sandwiched between layers of adhesive and electroded polyimide film. This film contains interdigitated electrodes that transfer the applied voltage directly to and from the ribbon shaped rods. This assembly enables in-plane poling, actuation, and sensing in a sealed, durable, ready-to-use package. When embedded in a surface or attached to flexible structures, the MFC provides distributed solid-state deflection and vibration control or strain measurements. While on display at a SPESIF-2009 exhibit booth, a P1 type advanced piezo-composite such as in Figure 9 repeatedly lifted an average-sized, half-pound orange. Therefore, its capability to quickly move the last critical magnet away from a stator position during rotor overshoot is another method to reduce detent and disengage the rotor at the end of the SMM cycle.

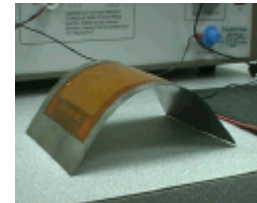


**FIGURE 9.** Piezo-Composite Actuator

### EXPERIMENTAL TRIALS

One problem with the spiral magnetic motor MAGLIM is designing the magnet alignment properly to maximize the circumferential force while minimizing the radial force. The general design consideration of using axial magnetic orientation emerged from FEMM simulations (*e.g.*, Figure 4c) for improving acceleration due to the magnetic gradient force while reducing the radial attraction of rotor to stator magnets. As noted above, a second part to this paper will explore the radial magnetic orientation designs for similar sized rotors.

### Work and Back Torque

The first series of MAGLIM models that were assembled and tested included NdFeB magnets (NdFeB 40, NdFeB 42 and NdFeB 50). The rotors and stators were constructed from hardwood with low permeable brass, stainless steel, acrylic and aluminum fittings. Figure 10 shows the six-inch rotor model at the equilibrium point at the end of a cycle with a 1” x 1.5” cylindrical rotor magnet. The spring latch at the bottom is designed to secure the *overshoot* which surprisingly, averaged about 45° or about  $\pi/4$  radians. The assembly on the left is an experimental counterweight that was also used for impact with a mirror-image of the same SMM above it on the same shaft for momentum exchange experiments. Mu metal shielding strips are seen at the track end.

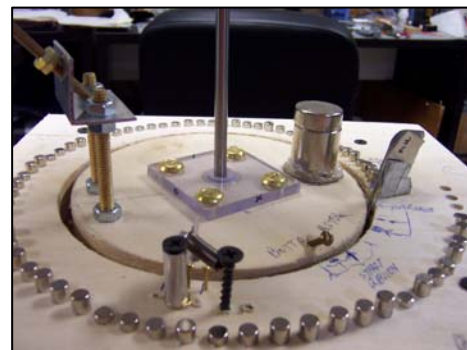


**FIGURE 10.** Photo of 6” rotor in the potential energy well at end of cycle.

The range of SMM models that were built includes 1.25, 3, 4, 6 and 10-inch diameter (Figure 11). It was found that using inches is convenient for hole saws. The measurement of back torque was made for all of the various rotor models. Figure 12 shows the basic linear slide Newton scale that was used for measuring back torque (4 inch model shown), ensuring that the scale was perpendicular to the radius of the rotor. The initial, maximum force to begin disengagement was recorded as an approximate measure of the work required as in equation (6). However, as further measurements were made closer to the potential well, at the end of the cycle, a gradual change in back torque occurs.

For example, with the 10-inch rotor model, the 45° section of arc between the latched final stop (see bottom of Figure 10) and the top of the potential hill which starts another cycle (clockwise from latch) was split into four equidistant subsections, about 11° each, for the 10-inch rotor. The torque exerted by the rotor was then measured at each location. In addition, the 275° section of arc between the top of the potential hill, marking the beginning of

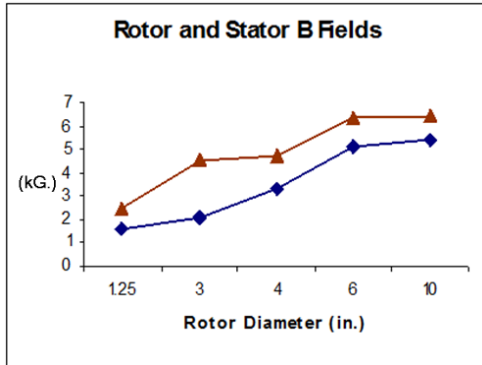


FIGURE 11. ▲ = rotor, ◆ = stator magnetic flux density.



FIGURE 12. Measuring back torque, Ohaus scale.

another cycle, and the bottom of the potential well, was also split into five convenient equidistant subsections, 55° each, with torque measurements made at each subsection. Not surprisingly, the force/torque measurements at each of the subsections were the same for four out of the five points, indicating a *successful design of a linearly increasing magnetic flux gradient* and a uniform angular acceleration. The results of the torque measurement are seen in Figure 13(b). The graph clearly shows the creation of back torque (positive torque) from 275° to 360°, the uniform forward torque (negative work) is also apparent from 0° to 275°. This is the first time such information has ever been measured for an SMM.

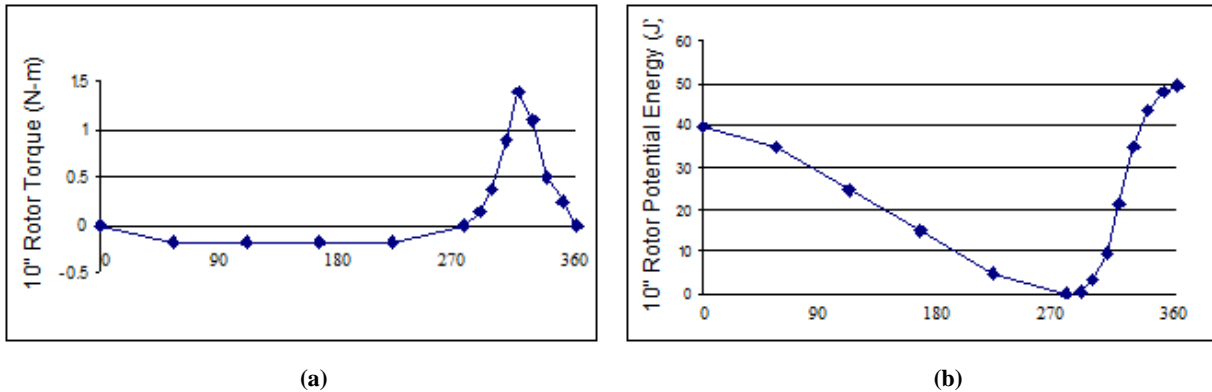
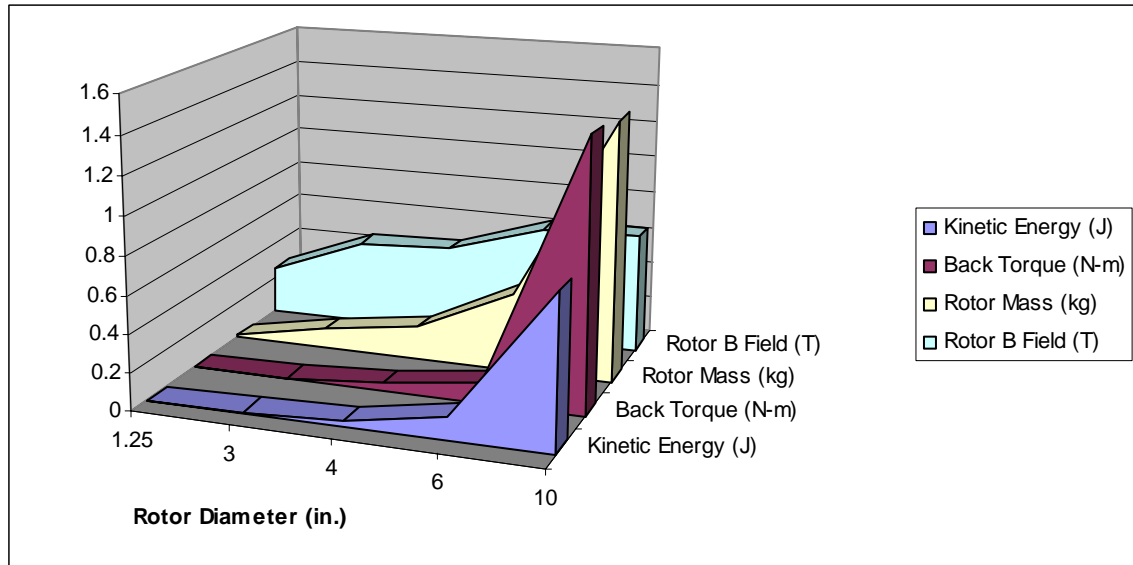


FIGURE 13. 10-inch rotor (a) torque and (b) potential energy versus angular displacement (degrees).

Furthermore, examining the values for the measured torque in Figure 13(a), it becomes apparent that they also represent the derivative at each point of the *potential energy curve* from equations (4) to (6). Such a potential energy curve, obtained by trapezoidal integration of the torque data points, is shown in Figure 13(b). Remarkably smooth, it decreases with a negative slope from 0° until reaching zero slope at the inflexion point of 275° which is an equilibrium point at the potential well. From 275° onwards, the potential energy  $U_B$  increases through overshoot region until reaching the maximum (steepest) derivative value at 315° where  $U_B$  continues to increase but with a decreasing slope (torque) until it levels out at the second inflexion point at 360° which corresponds to the maximum value for  $U_B$ . Further analysis on the energy balance can be done to determine the net work performed to move the rotor from the latched position of 315° to the top of the potential energy curve at 360°. Taking the force times distance, which for a rotating system is torque  $T$  integrated over the arc length  $d\theta$ , or  $W = \int T d\theta$  from equation (6), we find the amount of energy needed to overcome the last section of the SMM cycle.

The work done moving the 10-inch rotor from the latched point to the second inflexion point, using 0.77 radians for the angular displacement  $\theta$  region of interest, approximately equals 0.54 N-m or 0.54 joules. This value compares favorably with the peak kinetic energy measured for the 10-inch rotor of approximately 0.80 joules (as seen in Figure 14) based on rotor mass and angular velocity.



**FIGURE 14.** Comparison of the peak kinetic energy, peak back torque, rotor mass and rotor magnetic field for all of the five SMMs.

### **Rotor Mass, Angular Velocity, and Kinetic Energy**

As seen below, the peak kinetic energy measured for the 10-inch rotor is approximately 0.80 joules (Figure 14) based on rotor mass and angular velocity.

However, it is important to note that the 0.80 J of kinetic energy, which was calculated from the peak velocity, was consumed in climbing the potential hill from 275° to 315° where the rotor was latched into place, thus storing the accumulated kinetic energy before it is normally lost in the energy dissipative, oscillatory rebound which settles at the potential well. *Another 0.54 J of work energy is still needed*, according to the above calculation, for the rotor to pass from the 315° latch to the security of the 360° potential hill inflexion point in order to begin another cycle. The production of such an energy-equivalent in terms of the innovative suggestions from the previous section remains the focus of ongoing research in the SMM. Rotors with multiple magnets are also being tested as well as multiple rotors on the same shaft, in order to create a favorable energy production ratio.

More detailed information about the energy dynamics of the SMM in action was obtained by installing an interchangeable phototransistor harness above each of the SMMs and measuring the displacement versus time for one 5-cm and seven 10-cm intervals circumferentially around a 10-inch diameter circle, so as to accommodate every one of the SMMs. Each 10-cm circumferential displacement equals 0.787 radians or about 45°. Vishay BPW76B phototransistors with a TO-18 package were used with a transistor socket mounted horizontally at the appropriate positions. A centrally mounted light source was used to equally keep each PNP phototransistor in series with a 10K resistor in the on state and the output near ground. A thin, 1/16" thick brass rod, about the same thickness as the phototransistor window (Figure 15), was mounted securely on the perimeter of each rotor disk, rotating with the disk, to momentarily block the light and trigger a sharp pulse output of about 4 V which was sent into a computer programmed for data acquisition in BASIC. The program uses interval-halving to calculate the velocity for each interval and was originally applied to college physics student air track experiments for velocity and acceleration measurements. In this case, the circuitry was adapted to a circular arrangement around the periphery of the 10-inch harness with L-brackets made from aluminum screwed into acrylic with brass screw, all of which avoid disturbance of the magnetic fields due to their extremely low permeability.

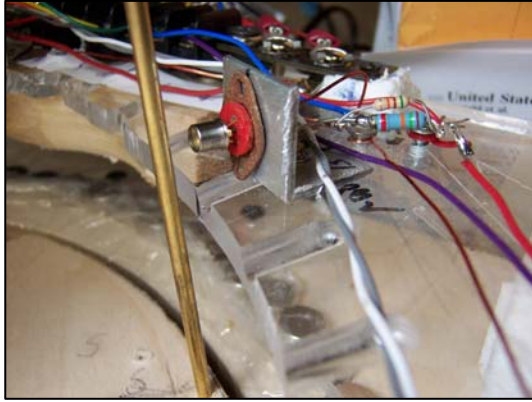


**FIGURE 15.** Phototransistor in place with vertical brass rod trigger passing by to block central light.

The multiple trials with each of the SMM 1.25, 3, 4, 6, and 10-inch rotor design models created repeatable but averaged data. As seen in Figure 14, the rotor magnetic flux density  $B$  varied from 0.25 T for the smallest rotor, to 0.45 T and 0.47 T for the 3" and 4" models respectively, and 0.63 T and 0.64 T for the 6" and 10" models respectively. All magnetic field measurements were made with an Integrity Design & Research gaussmeter, Model IDR-329. The results of the timed interval sampling during a single cycle of all of the SMMs are shown in Figure 16, along with a polynomial trend curve added for the 4" rotor data. What emerges from the data is the observation that the 3" and the 4" rotor models are the fastest of all of the models, actually reaching the fastest response time of the computer acquisition system. It is likely that the 3-radian data point of the 3" rotor should be closer to 18 rad/sec since 200 cm/sec (16 rad/sec) is the maximum speed that can be measured with the program due to the eight-bit processor. Otherwise, all of the other data points

are reliable and within a +/- 5% error tolerance. The small 1.25-inch (1" in the key for convenience) was the slowest rotor with the lowest  $B$  field and rotor mass as seen in Figure 14. However, interestingly, the 6" and the 10" rotors have almost identical angular velocity data, with the 10" rotor slowing down slightly as its potential well was well short of the end of the track (45° from the end vs. 25° from the end for the 6" rotor). If for no other reason, it is apparent from this insight that design efficiency and performance improvements can be achieved with the radial magnetic design for the next paper.

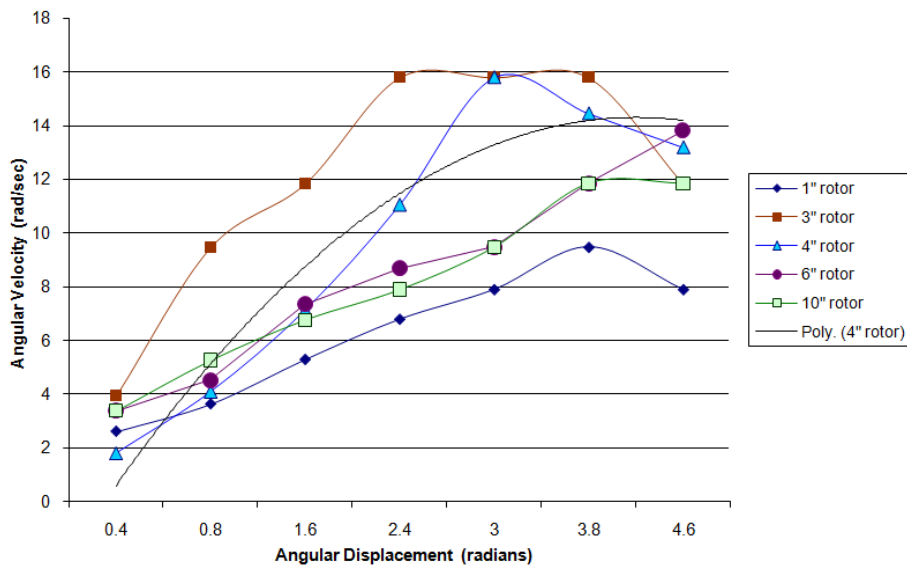


**FIGURE 16.** Computer acquired displacement data converted into angular velocity at each interval point for five different SMM designs with a polynomial trend line added for the 4-inch rotor.

Further observations made from a comparison of Figure 16 with Figure 14 yields the following correlation for future improvements. Figure 14 was designed as a composite graph in order to facilitate the comparison of parameters for each of the SMM designs. As seen above, the 6" and the 10" diameter rotor designs (Figure 16) performed most linearly with uniform acceleration, as well as the best trends toward a maximum velocity at the end of their cycle. Comparing them with Figure 14, it is noted that the rotor  $B$  fields are about the same. Furthermore, Figure 12 indicates the closest match between rotor and stator magnetic fields for the 6" and the 10" rotors as compared to the others. However, the rotor mass, back torque and kinetic energy are *maximized* with the 10" rotor, specifically where the rotor mass and back torque are on the same magnitude level. However, as seen from the in depth analysis of the 10" rotor, Figure 13, and the accompanying discussion, the rotor mass being so high for the 10" rotor, may well be

the single most important handicap preventing a more robust performance. Compared to the 10" rotor, the 6" rotor yielded 0.12 J of kinetic energy and about 0.11 N-m of back torque, which were on the same magnitude level, but its rotor mass was only 0.42 kg. Instead, the 10" rotor had its back torque of 1.4 N-m on the same magnitude level as the rotor mass (1.4 kg), with a much higher kinetic energy of 0.80 J. In other words, for about the same level of rotor B field (0.6 T), the 10" rotor achieved *6.7 times the maximum kinetic energy* with only 3.3 times the rotor mass as compared to the 6" rotor design, which shows an increase in efficiency, but it also suffered *13 times the maximum back torque* as the 6" rotor. This last statistic is perhaps due to the size of the rotor and stator magnets which were about twice the diameter as the 6" rotor and included a couple of one-inch NdFeB magnets sandwiched between two-inch by ½ inch NdFeB magnets, which are just about the largest and most powerful disk magnets commercially available. As a result, the magnetic coupling in the radial direction probably increased out of proportion to the circumferential improvement in angular velocity.

## Horsepower

Any motor analysis is not complete until the horsepower rating is determined. The power developed by each of the SMM is known with the product of angular velocity  $\omega$  and torque T to be (Granet, 1983),

$$P = T \omega \quad (11)$$

Therefore, for the 10" rotor SMM, we pick three sample data points from Figure 16 at 2.4, 3, and 3.8 radians for the calculation, each of which are increasing, though the torque (1.4 N-m) is known to be constant from Figure 13 ( $2\pi$  radians/360° conversion needed) in the region of interest.

$$P_{2.4} = 11 \text{ W} \quad P_{3.0} = 13 \text{ W} \quad P_{3.8} = 17 \text{ W} \quad (12)$$

Using 1 hp = 746 W we can therefore find that the fractional horsepower rating varies for these three regions of performance to be from 0.015 hp, 0.017 hp, up to 0.023 hp (about 1/43 hp) for the maximum rating.

## CONCLUSIONS

In conclusion, it has been demonstrated that the SMM can develop significant torque and horsepower, with about a half of a joule or 0.54 Watt-sec energy gap (equivalently 0.54 N-m torque gap), in the case of the largest 10" rotor SMM that was tested. It is also encouraging that magnetostatic energy density is thousands of times larger than electrostatic energy density. However, to close the gap, several creative boundary-changing methods have been proposed, one or more of which are needed to turn the tide of energy loss to energy gain. Halbach magnet arrays offer one-sided magnetic fields so that no field lines are wasted. The Hysteresis Motor design offers an improvement and an increase in negative torque or negative work. The MS-PZT pulser, the Wiegand pulse generator or the piezoelectric actuator are three major game changers that will have the biggest impact on the performance of the SMM since they can input energy where it is needed (at the end of the cycle) without any significant drain on the SMM angular velocity. It has been shown by the work of Ueno, Wiegand and others that *the proportion of external energy input required by physics for a magnetic field output energy pulse has recently become insignificantly small*. Therefore, it is predicted that future work in this area alone will yield enormous improvements to the point where break-even or actual energy production for the SMM can be foreseen, since exactly this type of switching-on of a powerful energy addition, with very little trigger input, has been used in the past to achieve a thermodynamically sound, optically controlled vacuum energy transducer (Pinto, 1999). Therefore, the use of a magnetically-triggered Barkhausen avalanche of magnetic domains providing a significant magnetic pulse with Wiegand modules for example, is seen to be a strategic advantage, with a larger energy impact than it takes to create it. The same is true for the piezoelectric options explored with electric charge triggering from a pickup coil. The future work with Toshiyuki Ueno from the University of Tokyo will explore the magnetic pulse capability of an SMM rotor-triggered MS-PZT device for realization of the proposed MAGLIM. As Ueno and Wiegand have proven, the amount of energy required to produce a given magnetic pulse can be dramatically reduced until it is insignificant. Thus, the converse must also be true: with prudent energy harvesting of the SMM kinetic energy in motion, along with an optimum design of a multi-magnet rotor SMM, a productively significant magnetic pulse can assist with the regauging requirements.

## NOMENCLATURE

$\beta$ = MacColl's constant	$\mu$ = permeability (gauss/oersted)
$\delta$ = thickness of plate (m)	$\mu_0$ = permeability of free space ( $4\pi \times 10^{-7}$ )
$\epsilon_0$ = $8.85 \times 10^{-12}$ (farad/m)	$S$ = spin quantum number of electron
$m$ = mass (kg)	$T$ = torque (N-m)
$\mu_s$ = electron magnetic moment ( $A\cdot m^2$ )	$U$ = potential energy (J)
$M$ = magnetic moment ( $A\cdot m^2$ )	$W$ = work (N-m or J)
$\rho$ = resistivity ( $\Omega\cdot m$ )	$\omega$ = angular velocity (rad/sec)
$\varphi$ = angle between magnetic moment and applied magnetic field	
$\theta$ = circumferential angular displacement (degrees or radians)	

## ACRONYMS

ESLIM	- Electrically Stimulated Linear Motor
hp	- horsepower
kG	- kilogauss
MAGLIM	- Magnetically Stimulated Linear Motor
MFC	- Macro Fiber Composite
MS	- magnetostrictive
N-m	- Newton-meters
NdFeB	- Neodymium-Iron-Boron
PZT	- piezoelectric
RPS	- revolutions per second
SMM	- spiral magnetic motor
SPESIF	- Space, Propulsion & Energy Sciences International Forum
T	- tesla
V	- volt or volts
W	- watts

## ACKNOWLEDGMENTS

Acknowledgement is given to H. Paul Sprain for soliciting my assistance with his spiral magnetic motor, to Toshiyuki Ueno for discovery of the zero power magnetic field generator, to Tom Schum for his SMM prototype, to John Wiegand for his amazing magnetic pulse wires and to Professor Eric Laithwaite, the inventor of the magnetically levitated train and hysteresis motor, whose tireless enthusiasm, published legacy and fascination with magnetic motors of all types has inspired many.

## REFERENCES

- Arrott, A. S., and Templeton, T. L., "Physical measurements in a permanent magnet field varying spatially," *J. App. Physics*, **99**, (2006), p. 08B507-1.
- Barkhausen, *Phys. Z.*, **20**(401), (1919).
- Bozorth, R. M., *Ferromagnetism*, J. Wiley & Sons, (2003), p. 786.
- Chikazumi, *Physics of Magnetism*, J. Wiley, (1964).
- Dilatush, Earle, "With No External Power Source, Clean Pulse-Generation Technique Creates Narrow, High-Level Outputs," EDN, Nov. 5, (1977), p. 19.
- Fujii, N., Kayasugat, T., and Hoshi, T., "Simple End Effect Compensator for Linear Induction Motor," *IEEE Trans on Magnetics*, V. 38, No. 5, 2002, p. 3264
- Gautreau, R. and Savin, W., *Modern Physics*, Schaum's Outline Series, McGraw-Hill Book Co., (1978), p. 120
- Granet, Irving, *Technical Mechanics*, Holt, Rinehart and Winston, (1983), p.320.
- Halliday, D. et al., *Physics*, John Wiley & Sons, Inc., (1962), p. 864.
- Hoburg, "Modeling Maglev Passenger Compartment Static Magnetic Fields from Linear Halbach Permanent-Magnet Arrays," *IEEE Trans. On Magnetics*, **40**(1), Jan., (2004), p. 59.
- Jang, S-M, Lee, S-H and Yoon, I-K, "Design Criteria for Detent Force Reduction of Permanent-Magnet Linear Synchronous Motors with Halbach Array," *IEEE Trans. On Magnetics*, **38**(5), (2002), p. 3261.
- Laithwaite, Eric, *Propulsion Without Wheels*, English Univ. Press, 1970.

- Niarchos, D., "Magnetic MEMS: key issues and some applications," *Sensors and Actuators A*, **109**, (2003), p. 166.
- Pinto, F., "Engine cycle of an optically controlled vacuum energy transducer," *Physical Review B*, **60**(21), 14, 740, 1999
- Scott, David, "Magnetic 'Wankel' for Electric Cars," *Popular Science*, June, (1979), p. 80.
- Ueno, T., Jinhaq, Q. and Junji, T., "Magnetic Force Control with Composite of Giant Magnetostrictive and Piezoelectric Materials," *IEEE Trans. On Magnetics*, **39**(6), (2003), p. 3534.
- Ueno, Toshiyuki, "Magnetic Force Control Based on the Inverse Magnetostrictive Effect," *IEEE Trans. Magnetics*, **40**(3), May, (2004), p. 1601.
- Ueno, Toshiyuki and Higuchi, Toshiro, "Zero-Power Magnetic Levitation Using Composite of Magnetostrictive/Piezoelectric Materials," *IEEE Trans. Magnetics*, **43**(8), Aug., (2007), p. 3477.
- Ueno et al., "Zero-Power Magnetic Levitation," *IEEE Trans. On Magnetics*, **43**(8), (2007), p. 3477.
- Valone, Thomas, "Eric Laithwaite Report: Gyromagnetic Engineering Genius, Publications, Inventions & News Clips," Integrity Research Institute, (2002).
- Valone, Thomas, "Is Permanent Magnetism Connected with Zero Point Energy?" *Zero Point Energy: The Fuel of the Future*, Integrity Research Institute, 1<sup>st</sup> edition, (2007), p. 200.